ICARUS **124,** 399–406 (1996)
ARTICLE NO. 0217

Asteroid Motions

MARK V. SYKES AND P. DANIEL MOYNIHAN

Steward Observatory, University of Arizona, Tucson, Arizona 85721
E-mail: sykes@as.arizona.edu

Received April 7, 1995; revised July 23, 1996

Equations are derived which describe the apparent motion of an asteroid traveling on an elliptical orbit in geocentric ecliptic coordinates. At opposition, the equations are identical to those derived by Bowell *et al.* (Bowell, E., B. Skiff, and L. Wasserman 1990. In *Asteroids, Comets, Meteors III* (C.-I. Lagerkvist, M. Rickman, B. A. Lindblad, and M. Lindgren, Eds.), pp. 19–24. Uppsala Universitet, Uppsala, Sweden). These equations can be an important component in the optimization of search strategies for specific asteroid populations based on their apparent motions relative to other populations when observed away from opposition. © 1996 Academic Press, Inc.

I. INTRODUCTION

Asteroid search programs look for objects near opposition, where coherent backscattering or other internal reflection effects contribute to a surge in brightness known as the opposition effect (Whitaker 1969, Hapke *et al.* 1993). However, many objects of particular interest may not be conveniently located at opposition, so some search programs strive for areal coverage. In addition, large area detectors, new scanning techniques, and the ability to store and process large volumes of data make possible increasingly efficient surveys over significant fractions of the available sky. Different programs have adopted different strategies, often complementary, in the search for near-Earth asteroids (NEAs). The Near-Earth Asteroid Tracking system (NEAT) observes about 100 square degrees per night near opposition, within 6 days on either side of the new moon each month (Helin *et al.* 1996). The proposed Lowell Observatory Near-Earth Object Search (LONEOS) will scan the entire available sky three times per month (Bowell *et al.* 1995). The Spacewatch program opts for lower areal coverage (3.3 square degrees every 1.5 hr) to detect fainter sources (Scotti 1993). The Bigelow Sky Survey scans the sky near opposition, but at ecliptic latitudes of 30° to 60° in order to filter for NEAs, comets, and high-inclination objects (Larson, personal communication).

Researchers often simulate asteroid motion numerically (e.g., Scotti 1993), but published equations describing ecliptic longitudinal and latitudinal motions of asteroids having arbitrary orbits are essentially restricted to the opposition point (Bowell *et al.* 1990). More generalized motion equations have been described (Jedicke 1996), but the focus here is on the development of an explicit and complete algebraic expression for the apparent latitudinal and longitudinal mo-

TABLE I
Definitions

λ	geometric ecliptic longitude
$\dot{\lambda}$	the time rate of change of geocentric ecliptic longitude
β	geocentric ecliptic latitude
$\dot{\beta}$	the time rate of change of geocentric ecliptic latitude
x	geocentric x-coordinate
y	geocentric y-coordinate
z	geocentric z-coordinate
$x_\odot$	heliocentric x-coordinate
$y_\odot$	heliocentric y-coordinate
$z_\odot$	heliocentric z-coordinate
$x_\oplus$	Earth's heliocentric x-coordinate
$y_\oplus$	Earth's heliocentric y-coordinate
$z_\oplus$	Earth's heliocentric z-coordinate
a	the semimajor axis of the orbit
e	the eccentricity of the orbit
i	inclination angle of the orbit to the ecliptic
Ω	longitude of the ascending node
ω	argument of perihelion
f	the true anomaly
r	$a(1 - e^2)/(1 + e \cos f)$ = heliocentric distance of the asteroid
q	$a(1 - e)$ = asteroid perihelion distance
ϕ	$(\omega + f)$ = angle between asteroid's position and the ascending node in its orbital plane (2π at opposition)
α	$\tan^{-1}(\tan \phi \cos i)$ = angle between the ascending node and a line from the Sun to the ecliptic plane above or below the asteroid's orbital position
u	$r(\sin^2 \phi \cos^2 i + \cos^2 \phi)^{1/2}$ = the projected heliocentric distance of an asteroid in the XY-plane
k	$\sqrt{GM_\odot}$ where G is the gravitational constant and $M_\odot$ is the mass of the Sun
R	Earth–Sun distance
$\Lambda_\oplus$	Earth's heliocentric longitude
$\dot{\Lambda}_\oplus$	motion of the Earth around the Sun

Note. All terms refer to asteroids unless otherwise specified.

0019-1035/96 $18.00
Copyright © 1996 by Academic Press, Inc.
All rights of reproduction in any form reserved.

tions of any object in an elliptical orbit viewed from the Earth, whether near or far from opposition. Such equations are useful tools for developing a better understanding of the expected motions of objects in the sky, understanding the relative motions of different asteroid populations, and designing search strategies for specific populations.

II. EQUATIONS OF APPARENT MOTION

Equations are derived in the Appendix for the apparent motion in geocentric ecliptic longitude ($\dot{\lambda}$) and latitude ($\dot{\beta}$) of an object in an arbitrary elliptical orbit. The equation variables are defined in Table I. The results are as follows:

$$\begin{aligned}\dot{\lambda} = {} & \frac{R\sin\Lambda_\oplus - u\sin(\Omega+\alpha)}{R^2+u^2-2Ru\cos(\Omega+\alpha-\Lambda_\oplus)} \\ & \times\left\{\left[\frac{eu\sin f\cos(\Omega+\alpha)}{1+e\cos f} - \frac{r^2}{u}\left(\sin(\Omega+\alpha)\cos i + \cos(\Omega+\alpha)\sin\phi\cos\phi\sin^2 i\right)\right]\sqrt{\frac{GM_\odot(1+e\cos f)}{r^3}} + (\sin\Lambda_\oplus)\sqrt{\frac{GM_\odot}{R}}\right\} \\ & - \frac{R\cos\Lambda_\oplus - u\cos(\Omega+\alpha)}{R^2+u^2-2Ru\cos(\Omega+\alpha-\Lambda_\oplus)} \\ & \times\left\{\left[\frac{eu\sin f\sin(\Omega+\alpha)}{1+e\cos f} + \frac{r^2}{u}\left(\cos(\Omega+\alpha)\cos i - \sin(\Omega+\alpha)\sin\phi\cos\phi\sin^2 i\right)\right]\sqrt{\frac{GM_\odot(1+e\cos f)}{r^3}} - (\cos\Lambda_\oplus)\sqrt{\frac{GM_\odot}{R}}\right\}.\end{aligned} \tag{1}$$

To convert longitudinal motion to the component of angular motion along a line of constant latitude, $\dot{\lambda}$ must be weighted by $\cos\beta$.

$$\begin{aligned}\dot{\beta} = {} & \frac{[R\cos\Lambda_\oplus - u\cos(\Omega+\alpha)](r\sin\phi\sin i)}{[r^2+R^2-2uR\cos(\Omega+\alpha-\Lambda_\oplus)]\sqrt{u^2+R^2-2uR\cos(\Omega+\alpha-\Lambda_\oplus)}} \\ & \times\left\{\left[\frac{eu\sin f\cos(\Omega+\alpha)}{1+e\cos f} - \frac{r^2}{u}\left(\sin(\Omega+\alpha)\cos i + \cos(\Omega+\alpha)\sin\phi\cos\phi\sin^2 i\right)\right]\sqrt{\frac{GM_\odot(1+e\cos f)}{r^3}} + (\sin\Lambda_\oplus)\sqrt{\frac{GM_\odot}{R}}\right\} \\ & + \frac{[R\sin\Lambda_\oplus - u\sin(\Omega+\alpha)](r\sin\phi\sin i)}{[r^2+R^2-2uR\cos(\Omega+\alpha-\Lambda_\oplus)]\sqrt{u^2+R^2-2uR\cos(\Omega+\alpha-\Lambda_\oplus)}} \\ & \times\left\{\left[\frac{eu\sin f\sin(\Omega+\alpha)}{1+e\cos f} - \frac{r^2}{u}\left(\cos(\Omega+\alpha)\cos i - \sin(\Omega+\alpha)\sin\phi\cos\phi\sin^2 i\right)\right]\sqrt{\frac{GM_\odot(1+e\cos f)}{r^3}} - (\cos\Lambda_\oplus)\sqrt{\frac{GM_\odot}{R}}\right\} \\ & + \frac{r\sin i\sqrt{u^2+R^2-2uR\cos(\Omega+\alpha-\Lambda_\oplus)}}{r^2+R^2-2uR\cos(\Omega+\alpha-\Lambda_\oplus)}\left[\cos\phi + \frac{e\sin\phi\sin f}{1+e\cos f}\right]\sqrt{\frac{GM_\odot(1+e\cos f)}{r^3}}.\end{aligned} \tag{2}$$

At opposition the Sun, Earth, and asteroid are collinear and the asteroid is at its ascending node. Therefore,

$$\phi = \omega + f = 2\pi \tag{3}$$

$$\alpha = 0 \tag{4}$$

$$\Lambda_\oplus = \Omega. \tag{5}$$

Substituting the above into (1) and (2) yields

$$\dot{\lambda} = \frac{k}{r-R}\left(\frac{1}{r}\sqrt{a(1-e^2)}\cos i - \frac{1}{\sqrt{R}}\right) \tag{6}$$

$$|\dot{\beta}| = \frac{k}{r(r-R)}\sqrt{a(1-e^2)}\sin i. \tag{7}$$

A comparison with the results of Bowell *et al.* (1990) yields identical equations for asteroid motion at opposition when $R = 1$.

III. MOTIONS OF SAMPLE POPULATIONS

Synthetic asteroid populations loosely representing the Atens, near-Earth asteroids (NEAs), and inner main belt asteroids (IMBs) are chosen for illustrating characteristic motions of different asteroid populations. They were defined in orbital element space by their semi-major axes, a, eccentricities, e, and orbital inclinations, i, and are listed

TABLE II
Simulated Asteroid Populations

	a (AU)	e	i (°)	
Atens	0.7–1.0	0.01–0.8	0–60	
NEAs	$a > 1$	0.01–0.8	0–60	$q < 1.3$ AU
Inner main belt	2.15–2.5	0.025–0.3	0–9	

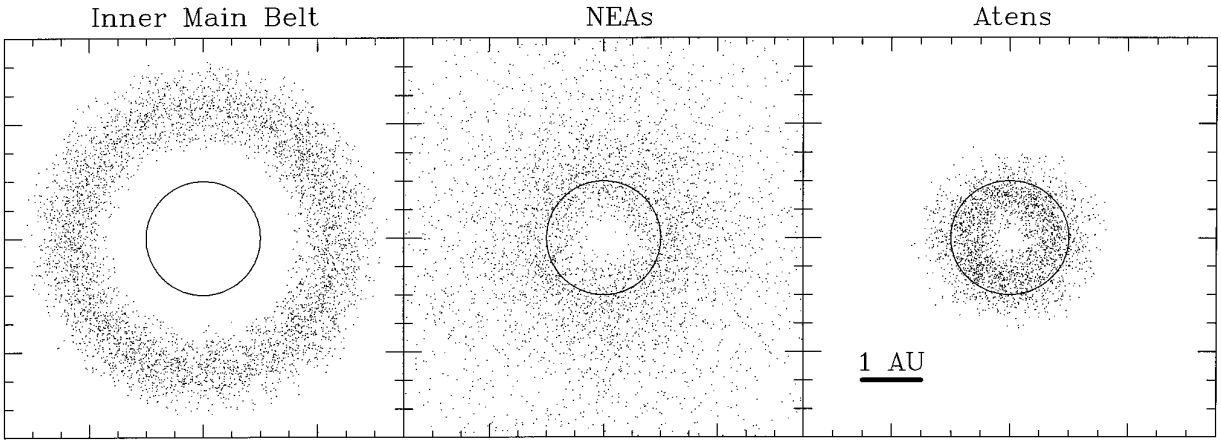

FIG. 1. Random asteroid positions selected for simulated Atens, near-Earth asteroids (NEAs), and inner main belt asteroids. The Earth's orbit is shown for scale.

in Table II. The other orbital elements, ω, Ω, and f, were allowed to vary between 0 and 360 degrees. These element distributions are not meant to be the "true" distributions of those specific populations, but rather are representative of the ranges associated with them, thus serving as a means of exploring the potential range of apparent motions that they may exhibit.

Toward this end, positions and motions of objects within a population were determined by randomly sampling over their range of elements. All calculations assume the Earth at 0° ecliptic longitude and the objects in prograde orbits. Figure 1 shows the positions of asteroids within each sample population examined.

Because of parallax effects, motions of asteroids of a given population will depend on the location of the sky at which they are observed. In Fig. 2 we show a schematic of the different areas sampled in geocentric ecliptic coordinates. Each population is distributed within a torus which we assume to be Sun-centered (forced eccentricity of zero) and with a plane of symmetry coinciding with the ecliptic (forced inclination of zero). As a result, the distribution of asteroid motions will be symmetric above and below the ecliptic and on either side of opposition in longitude.

In Fig. 3 we show the distribution of motions for each population in each of the spatial regions of Fig. 2, including the special case of apparent motion at opposition. The greatest amplitude of motions is exhibited by the population whose members can pass closest to the Earth, maximizing the effects of parallax. These are the Atens. As we consider populations more distant from the Earth and Sun, ranges of motions systematically decrease.

At the opposition point, the motion of the Earth results in the longitudinal motions of the asteroids largely appearing retrograde, due to their typically lower orbital

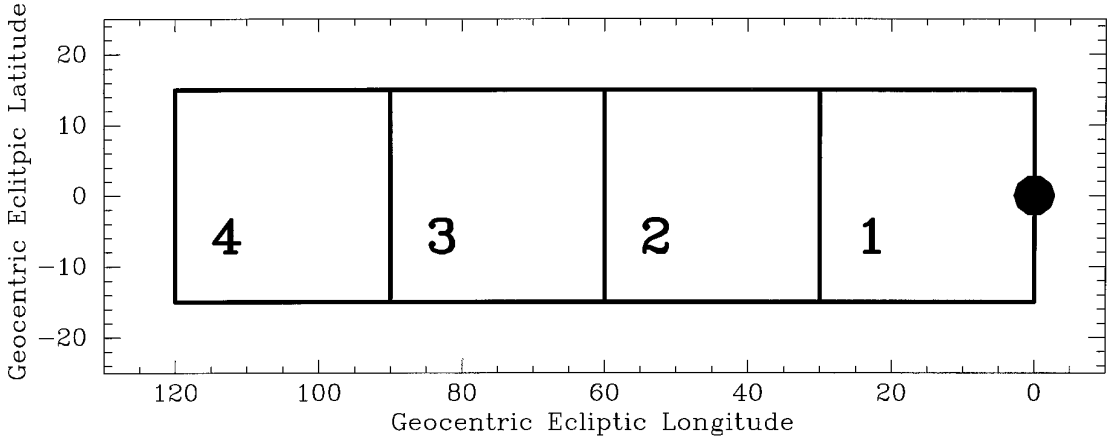

FIG. 2. Sampling regions on the sky centered on the ecliptic. The assumed opposition point is marked by the dot.

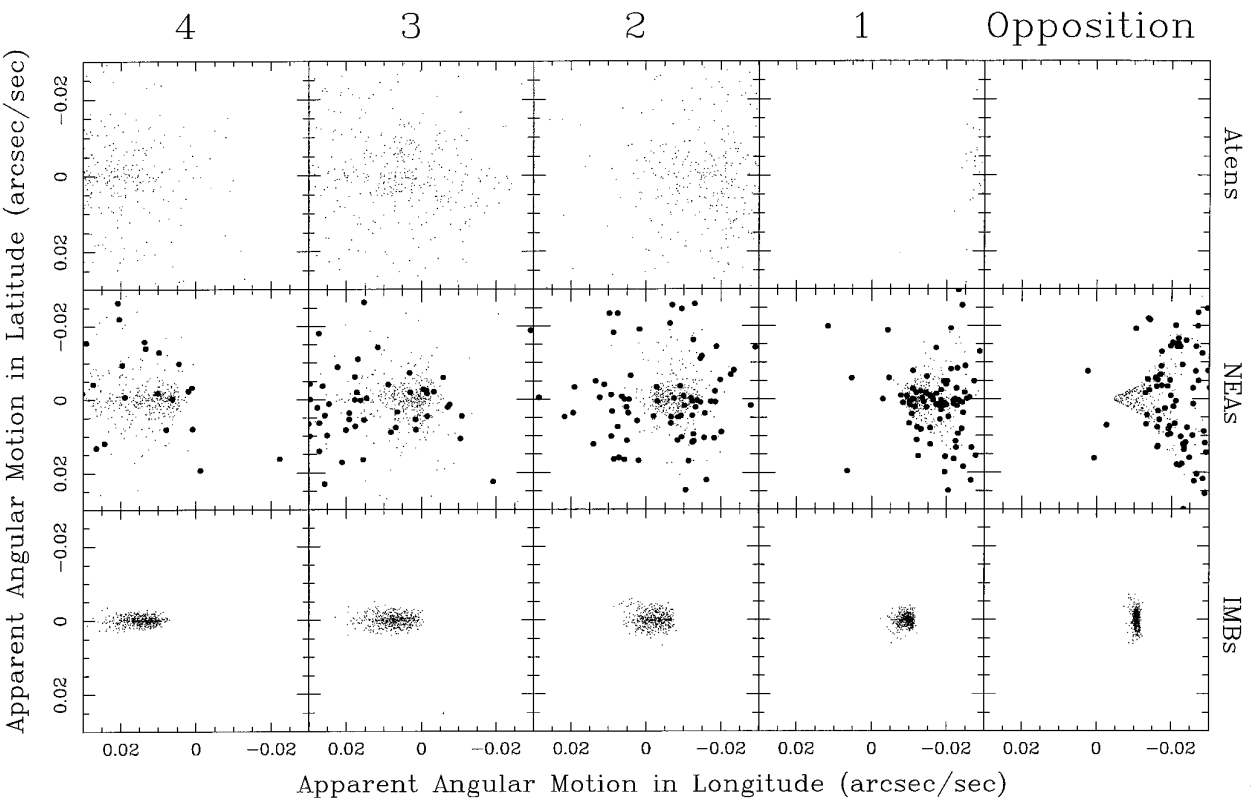

FIG. 3. Apparent motion of Atens, near-Earth asteroids (NEAs), and inner main belt asteroids (IMBs) at opposition and within designated regions of the sky at progressively increasing distances in ecliptic longitude away from the opposition point (see Fig. 3). Apparent motion in longitude corresponds to $\dot{\lambda} \cos \beta$. Heavy dots correspond to brighter NEAs (see text). Simulations were run until 500 objects of each population were found in each region. In some cases the range of angular motions of objects exceeds the rates spanned by this figure. This is the case for all Atens at opposition, which were retrograde.

speed. In Fig. 3, as we move away from the opposition point this is less and less the case, due to the foreshortening of the Earth's motion vector in the direction of the asteroids, until asteroid angular motions are almost all prograde as we look in the direction (or anti-direction) of the Earth's motion.

There is a degree of circularity in designing a search program to maximize the probability of finding members of a specific population of asteroids, as we begin with a model of what we expect to find. Success depends in part on the accuracy of that model. One must also model the population of background asteroids against which the target population may be observed.

Asteroids at high ecliptic latitudes will most likely be members of near-Earth and Earth-crossing populations. Near the ecliptic, apparent magnitude can also be a factor in distinguishing model populations. We further characterized our NEAs by assuming a geometric albedo of 0.2, a slope parameter of 0.25, and a cumulative size–frequency index of 2.5 (comparable to a collisionally relaxed population) with a minimum diameter of 0.1 km. Diameters were randomly assigned in a way that reproduces the above distribution. Apparent visual magnitudes were then calculated using the two-parameter IAU magnitude system described by Bowell *et al.* (1989) (Fig. 4).

In Fig. 3, NEAs having magnitudes brighter than 23 were shown as heavier dots. These objects show a greater range of apparent motion because of their closer proximity to the Earth (the bright slow moving objects are larger members seen at greater distances). However, as more distant fainter objects are observed, their motions tend to cluster over a narrower, slower range with the result that in some areas of the sky (e.g., regions 1, 2, 3 in Fig. 2) the motions of an increasing fraction of fainter NEAs tend to be indistinguishable from the more populous inner main belt objects. In other areas of the sky (e.g., at opposition and region 4 in Fig. 2) it appears that the bulk of faint NEAs may be distinguished from IMBs by their *lower* characteristic apparent motions. However, comparison with the motions of simulated outer main belt and Trojan asteroids indicate that faint NEAs would not be distinguishable from those more distant objects. We point out, however, that there are still increasing numbers of NEAs exhibiting anomalous motion as searchers go fainter and fainter.

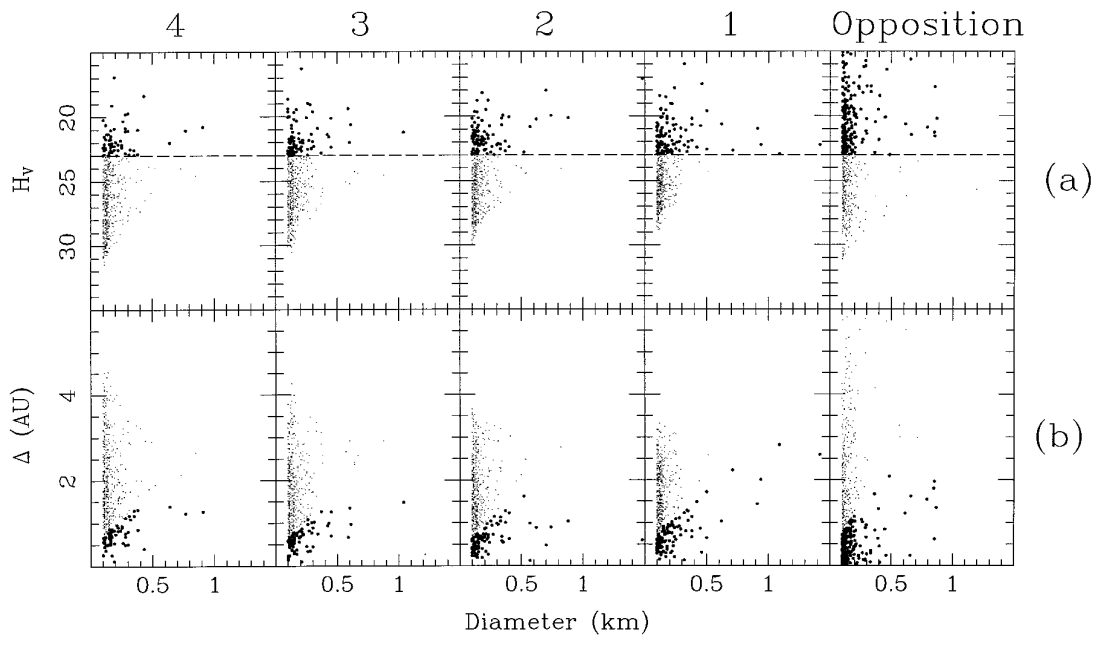

FIG. 4. (a) Apparent visual magnitude, H_V, and (b) geocentric distance, Δ, of NEAs as a function of diameter for 500 objects in each region of Fig. 3. Heavy dots denote objects having magnitudes lower (hence brighter) than 23.

IV. CONCLUSIONS

It is clear that different asteroid populations will have distinctive distributions of angular motions which vary depending on where in the sky they are being observed. By combining this information with other model assumptions for the sizes, albedo, and other surface scattering properties of different populations, search strategies focussing on specific populations can be explored.

Application of the equations of apparent asteroid motion along with equations for position in the Appendix yield some general results that are well-known to those conducting asteroid search programs. This includes the fact that above 25° ecliptic latitude, the number density of main belt asteroids diminishes rapidly, greatly increasing the probability that a given detection is an NEA. Also, the increasing confusion in distiguishing between NEAs and mainbelt asteroids on the basis of their apparent motions as one searches for fainter objects argues for the validity of search strategies which cover large areas of sky to find the brightest members of that population exhibiting anomolous motion in addition to searchers for fainter objects over smaller areas.

APPENDIX: DERIVING $\dot{\lambda}$ AND $\dot{\beta}$

We begin by considering the position of an asteroid in space, relative to the Earth and Sun in rectangular coordinates. From Fig. 5,

$$x = x_\odot - x_\oplus \tag{A1}$$

$$y = y_\odot - y_\oplus \tag{A2}$$

$$z = z_\odot - z_\oplus. \tag{A3}$$

The motion of the asteroid along each axis is

$$\frac{dx}{dt} = \frac{dx_\odot}{df}\frac{df}{dt} - \frac{dx_\oplus}{dt} \tag{A4}$$

$$\frac{dy}{dt} = \frac{dy_\odot}{df}\frac{df}{dt} - \frac{dy_\oplus}{dt} \tag{A5}$$

$$\frac{dz}{dt} = \frac{dz_\odot}{df}\frac{df}{dt} - \frac{dz_\oplus}{dt}. \tag{A6}$$

The time rate of change of geocentric ecliptic longitude of an asteroid may be expressed as

$$\dot{\lambda} = \frac{d\lambda}{dx}\frac{dx}{dt} + \frac{d\lambda}{dy}\frac{dy}{dt} + \frac{d\lambda}{dz}\frac{dz}{dt}, \tag{A7}$$

where $d\lambda/dz$ is always zero. Substituting (A4) and (A5) into (A7) gives

$$\dot{\lambda} = \frac{d\lambda}{dx}\left(\frac{dx_\odot}{df}\frac{df}{dt} - \frac{dx_\oplus}{dt}\right) + \frac{d\lambda}{dy}\left(\frac{dy_\odot}{df}\frac{df}{dt} - \frac{dy_\oplus}{dt}\right) + 0. \tag{A8}$$

Similarly, the time rate of change of geocentric ecliptic latitude of an asteroid is

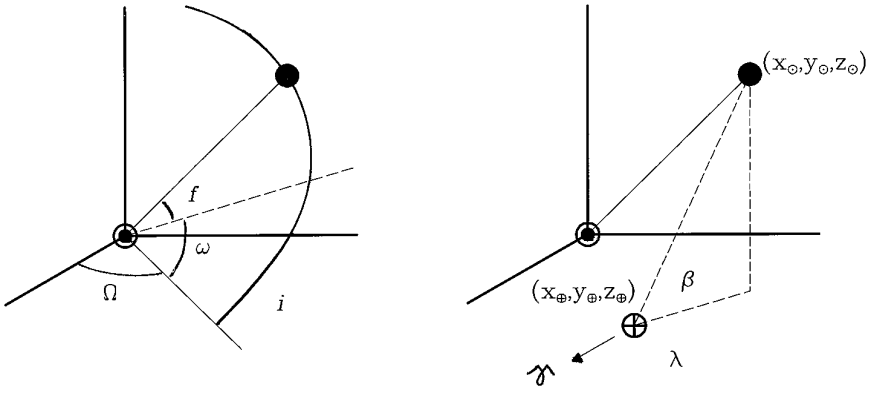

FIG. 5. Geometry of asteroid motion.

$$\dot{\beta} = \frac{d\beta}{dx}\frac{dx}{dt} + \frac{d\beta}{dy}\frac{dy}{dt} + \frac{d\beta}{dz}\frac{dz}{dt}. \tag{A9}$$

Substituting (A4)–(A6) into (A9),

$$\dot{\beta} = \frac{d\beta}{dx}\left(\frac{dx_\odot}{df}\frac{df}{dt} - \frac{dx_\oplus}{dt}\right) + \frac{d\beta}{dy}\left(\frac{dy_\odot}{df}\frac{df}{dt} - \frac{dy_\oplus}{dt}\right) + \frac{d\beta}{dz}\left(\frac{dz_\odot}{df}\frac{df}{dt} - \frac{dz_\oplus}{dt}\right), \tag{A10}$$

where $dz_\oplus/dt$ is always zero. In the following sections, the each of the individual terms of (A8) and (A10) will be derived.

First, the heliocentric rectangular and ecliptic coordinates of an asteroid are given in terms of its orbital elements. From Fig. 5, the projected heliocentric distance of the asteroid in the XY-plane is given by

$$u = r(\sin^2\phi\cos^2 i + \cos^2\phi)^{1/2}. \tag{A11}$$

We can use this side to solve for the $x_\odot$ and $y_\odot$ coordinates. Again, from Fig. 1,

$$x_\odot = u\cos(\Omega+\alpha) = \frac{a(1-e^2)}{1+e\cos f}(\sin^2\phi\cos^2 i + \cos^2\phi)^{1/2}\cos(\Omega+\alpha). \tag{A12}$$

Similarly, for $y_\odot$

$$y_\odot = u\sin(\Omega+\alpha) = \frac{a(1-e^2)}{1+e\cos f}(\sin^2\phi\cos^2 i + \cos^2\phi)^{1/2}\sin(\Omega+\alpha). \tag{A13}$$

Finally, we determine $z_\odot$,

$$z_\odot = r\sin\phi\sin i \tag{A14}$$

$$= \frac{a(1-e^2)}{1+e\cos f}\sin\phi\sin i. \tag{A15}$$

Now the heliocentric ecliptic coordinates may be calculated:

$$\lambda_\odot = \tan^{-1}\left(\frac{y_\odot}{x_\odot}\right) = \tan^{-1}\left(\frac{\sin(\Omega+\alpha)}{\cos(\Omega+\alpha)}\right) = \Omega+\alpha \tag{A16}$$

and

$$\beta_\odot = \tan^{-1}\left(\frac{z_\odot}{\sqrt{x_\odot^2+y_\odot^2}}\right) = \tan^{-1}\left(\frac{\sin\phi\sin i}{\sqrt{\sin^2\phi\cos^2 i+\cos^2\phi}}\right). \tag{A17}$$

Next, we derive the rate of change of the heliocentric rectangular coordinates of the asteroid with change in its true anomaly ($dx_\odot/df$, $dy_\odot/df$, and $dz_\odot/df$). Rewriting (A12) yields

$$x_\odot = a(1-e^2)\frac{u_1u_2}{v}, \tag{A18}$$

where

$$u_1 = (\sin^2\phi\cos^2 i + \cos^2\phi)^{1/2}, \tag{A19}$$

$$u_2 = \cos(\Omega+\alpha), \tag{A20}$$

and

$$v = 1 + e\cos f. \tag{A21}$$

Using the quotient rule yields

$$\frac{dx_\odot}{df} = a(1-e^2)\frac{(u_1\,du_2 + u_2\,du_1)v - u_1u_2\,dv}{v^2\,df}, \tag{A22}$$

where their differentials are given by

$$du_1 = -\frac{\sin\phi\cos\phi\sin^2 i}{u_1}df \tag{A23}$$

$$\begin{aligned} du_2 &= -\sin(\Omega + \alpha)\, d\alpha \\ &= -\sin(\Omega + \alpha)\frac{\cos i}{u_1^2}\, df \end{aligned} \tag{A24}$$

$$dv = -e \sin f\, df. \tag{A25}$$

Substituting (A19)–(A21) and (A23)–(A24) into (A22) yields

$$\begin{aligned} \frac{dx_\odot}{df} = &-\frac{r^2}{u}[\sin(\Omega + \alpha)\cos i + \cos(\Omega + \alpha)\sin\phi\cos\phi\sin^2 i] \\ &+ \frac{eu\sin f\cos(\Omega + \alpha)}{1 + e\cos f}. \end{aligned} \tag{A26}$$

Next we derive $dy_\odot/df$. Rewriting (A13) yields

$$y_\odot = a(1 - e^2)\frac{u_1 u_3}{v}, \tag{A27}$$

where u_1 is defined by (A19), v by (A12), and

$$u_3 = \sin(\Omega + \alpha). \tag{A28}$$

Using the quotient rule,

$$\frac{dy_\odot}{df} = a(1 - e^2)\frac{(u_1\, du_3 + u_3\, du_1)v - u_1 u_3\, dv}{v^2}, \tag{A29}$$

where du_1 is given by (A23) and dv by (A25), and

$$\begin{aligned} du_3 &= \cos(\Omega + \alpha)\, d\alpha \\ &= \cos(\Omega + \alpha)\frac{\cos i}{u_1^2}\, df. \end{aligned} \tag{A30}$$

Substituting Eqs. (A19), (A21), (A23), (A25), (A28), and (A30) back into (A29) yields

$$\begin{aligned} \frac{dy_\odot}{df} = &\frac{r^2}{u}[\cos(\Omega + \alpha)\cos i - \sin(\Omega + \alpha)\sin\phi\cos\phi\sin^2 i] \\ &+ \frac{eu\sin f\sin(\Omega + \alpha)}{1 + e\cos f}. \end{aligned} \tag{A31}$$

Finally, we derive $dz_\odot/df$. From (A15),

$$\frac{dz_\odot}{df} = r\sin i\left[\cos\phi + \frac{e\sin\phi\sin f}{1 + e\cos f}\right]. \tag{A32}$$

Next we take into account the motion of the Earth and determine the geocentric rectangular coordinates for an asteroid (x, y, z). Assume that the Earth is in a circular orbit of radius R. Its position is given by

$$x_\oplus = R\cos\Lambda_\oplus \tag{A33}$$

$$y_\oplus = R\sin\Lambda_\oplus \tag{A34}$$

$$z_\oplus = 0, \tag{A35}$$

where $\Lambda_\oplus$ is determined by the date. The angular motion of the Earth is

$$\dot\Lambda_\oplus = \sqrt{\frac{GM_\odot}{R^3}}. \tag{A36}$$

The rate of change of the heliocentric x-coordinate of the Earth is given by

$$\dot x_\oplus = \frac{dx_\oplus}{dt} = -R\dot\Lambda_\oplus\sin\Lambda_\oplus. \tag{A37}$$

The rate of change of the heliocentric y-coordinate of the Earth is given by

$$\dot y_\oplus = \frac{dy_\oplus}{dt} = R\dot\Lambda_\oplus\cos\Lambda_\oplus. \tag{A38}$$

Now, from Eqs. (A1)–(A3), (A33), and (A34),

$$x = u\cos(\Omega + \alpha) - R\cos\Lambda_\oplus \tag{A39}$$

$$y = u\sin(\Omega + \alpha) - R\sin\Lambda_\oplus \tag{A40}$$

$$z = r\sin\phi\sin i. \tag{A41}$$

Next, we will determine the rates of change of an asteroid's geocentric ecliptic coordinates with change in geocentric rectangular coordinates ($d\lambda/dx, d\lambda/dy, d\beta/dx, d\beta/dy$, and $d\beta/dz$). The geocentric ecliptic longitude of an asteroid is expressed in geocentric rectangular coordinates by

$$\lambda = \tan^{-1}\left(\frac{y}{x}\right). \tag{A42}$$

Thus,

$$\frac{d\lambda}{dx} = \frac{-y}{x^2 + y^2} = \frac{-u\sin(\Omega + \alpha) + R\sin\Lambda_\oplus}{R^2 + u^2 - 2Ru\cos(\Omega + \alpha - \Lambda_\oplus)}. \tag{A43}$$

Similarly,

$$\frac{d\lambda}{dy} = \frac{x}{x^2 + y^2} = \frac{u\cos(\Omega + \alpha) - R\cos\Lambda_\oplus}{R^2 + u^2 - 2Ru\cos(\Omega + \alpha - \Lambda_\oplus)}. \tag{A44}$$

The geocentric ecliptic latitude is expressed by

$$\beta = \tan^{-1}(w), \tag{A45}$$

where

$$w = \frac{z}{\sqrt{x^2 + y^2}}. \tag{A46}$$

Thus,

$$\begin{aligned} \frac{d\beta}{dx} &= \frac{d\beta}{dw}\frac{dw}{dx} \\ &= -\frac{xz}{(x^2 + y^2 + z^2)\sqrt{x^2 + y^2}} \\ &= \frac{[R\cos\Lambda_\oplus - u\cos(\Omega + \alpha)](r\sin\phi\sin i)}{[r^2 + R^2 - 2uR\cos(\Omega + \alpha - \Lambda_\oplus)]\sqrt{u^2 + R^2 - 2uR\cos(\Omega + \alpha - \Lambda_\oplus)}}, \end{aligned} \tag{A47}$$

$$\frac{d\beta}{dy} = \frac{d\beta}{dw}\frac{dw}{dy}$$

$$= -\frac{yz}{(x^2+y^2+z^2)\sqrt{x^2+y^2}}$$

$$= \frac{[R\sin\Lambda_\oplus - u\sin(\Omega+\alpha)](r\sin\phi\sin i)}{[r^2+R^2-2uR\cos(\Omega+\alpha-\Lambda_\oplus)]\sqrt{u^2+R^2-2uR\cos(\Omega+\alpha-\Lambda_\oplus)}}, \quad \text{(A48)}$$

and

$$\frac{d\beta}{dz} = \frac{d\beta}{dw}\frac{dw}{dz}$$

$$= \frac{\sqrt{x^2+y^2}}{x^2+y^2+z^2} \quad \text{(A49)}$$

$$= \frac{\sqrt{u^2+R^2-2uR\cos(\Omega+\alpha-\Lambda_\oplus)}}{r^2+R^2-2uR\cos(\Omega+\alpha-\Lambda_\oplus)}.$$

Lastly, the variation of the true anomaly with time is derived from conservation of angular momentum and is given by

$$\dot{f} = \sqrt{\frac{GM_\odot(1+e\cos f)}{r^3}}. \quad \text{(A50)}$$

Substituting Eqs. (A26), (A31), (A37), (A38), (A43), (A44), and (A50) into Eq. (A8) we are able to solve for the motion in geocentric longitude, $\dot{\lambda}$, the result of Eq. (1) in the text.

Substituting Eqs. (A26), (A31), (A32), (A37), (A38), (A47), (A48), (A49), and (A50) into Eq. (A10) we are able to solve for the motion in geocentric latitude, $\dot{\beta}$, the result of Eq. (2) in the text.

ACKNOWLEDGMENTS

The authors thank E. Bowell, R. Jedicke, and J. Scotti for their comments and discussions from which this work has benefitted. We also thank A. Harris and D. Mink for their helpful reviews.

REFERENCES

Bowell, E., B. Skiff, and L. Wasserman 1990. In *Asteroids, Comets, Meteors III* (C.-I. Lagerkvist, M. Rickman, B. A. Lindblad, and M. Lindgren, Eds.), pp. 19–24. Uppsala Universitet, Uppsala, Sweden.

Bowell, E., B. Koehn, S. Howell, H. Hoffman, and K. Muinonen 1995. The Lowell Observatory Near-Earth-Object Search: A progress report. *Bull. Am. Astron. Soc.* **95,** 1057.

Bowell, E., B. Hapke, D. Domingue, K. Lumme, J. Peltoniemi, and A. Harris 1989. Application of photometric models to asteroids. In *Asteroids II* (R. Binzel, T. Gehrels, and M. Matthews, Eds.), pp. 524–556. Univ. of Arizona Press, Tuscon.

Hapke, B., R. Nelson, and W. Smythe 1993. The opposition effect of the Moon: The contribution of coherent backscatter. *Science* **260,** 509–511.

Helin, E., S. Pravdo, K. Lawrence, and the JPL NEAT/Air Force GEODSS Teams 1996. Jet Propulsion Laboratory's near-Earth asteroid tracking (NEAT) program: Now operational, producing exciting new NEOs. In *Asteroids, Comets, Meteors*, in press.

Jedicke, R. 1996. Detection of near Earth asteroids based upon their rates of motion. *Astron. J.* **111,** 970–982.

Scotti, J. 1994. Computer aided near Earth object identification. In *Asteroids, Comets, Meteors 1993* (A. Milani *et al.*, Eds.), pp. 17–30. IAU.

Whitaker, E. 1969. An investigation of the lunar heiligenschein. In *Analysis of Apollo 8 Photometry and Visual Observations*, NASA SP-201, pp. 38–39. NASA.